Role of Self-Heating and Polarization in AlGaN/GaN Based Heterostructures

K. Ahmeda, B. Ubochi, B. Benbakhti, S. J. Duffy, A. Soltani, W. Zhang, and K. Kalna

***Abstract*—The interplay of self-heating and polarization affecting resistance is studied in AlGaN/GaN Transmission Line Model (TLM) heterostructures with a scaled source-to-drain distance. The study is based on meticulously calibrated TCAD simulations against I-V experimental data using an electro-thermal model. The electro-thermal simulations show hot-spots (with peak temperature in a range of $\sim$ 566 K - 373 K) at the edge of the drain contact due to a large electric field. The electrical stress on Ohmic contacts reduces the total polarization, leading to the inverse/converse piezoelectric effect. This inverse effect decreases the polarization by 7 %, 10 %, and 17 % during a scaling of the source-to-drain distance in the 12 μm, 8 μm and 4 μm TLM heterostructures, respectively, when compared to the largest 18 μm heterostructure.**

***Index Terms*—III-V Nitrides, Self-Heating, Polarization, TLM Structures, Electro-Thermal Transport Simulations.**

I. Introduction

GALLIUM Nitride (GaN) wide bandgap material possesses attractive properties such as a high breakdown electric field of 3.3 MV/cm, a large carrier mobility in two-dimensional electron gas (2DEG) of 2000 $cm^2/V.s$, a large saturation velocity of 2.5×10^7 cm/s, a large energy bandgap of 3.4 eV, a low relative permittivity of 10.4, and a high thermal conductivity (κ) of 130 $Wm^{-1}K^{-1}$ [1], [2]. In addition, III-Nitride based semiconductors possess a large polarization, which is the result of an asymmetrical distribution of electron clouds. Therefore, spontaneous and piezoelectric polarizations play a vital role in AlGaN/GaN heterostructure based devices. The polarization together with a large band discontinuity at the AlGaN/GaN heterostructure interface lead to a very effective creation of a 2DEG [3]. All these properties offer a range of options to design highly effective power electronics devices using concept of High Electron Mobility Transistors (HEMTs), which are urgently required for variety of future power and high frequency in electronic applications [4]–[6].

In this paper, we study electro-thermal behavior of scaled AlGaN/GaN Transmission Line Model (TLM) heterostructures with low resistive Ohmic contacts aimed for AlGaN/GaN HEMTs. Understanding the physical transport process in the contacts is crucial for the following reasons: (1) reducing on-resistance to minimize power loss in Ohmic contacts and (2) achieving a higher extrinsic transconductance (g_m) resulting in the increment of current gain and cut-off frequency [7]. The fabrication and specification of AlGaN/GaN TLM heterostructures is described in Section II. Sections III and IV outline the simulation methodology and the impact of both self-heating and polarization effects on the device performance. Conclusions are drawn in Section V.

K. Ahmeda, B. Ubochi, and K. Kalna are with Nanoelectronic Devices Computational Group, College of Engineering, Swansea University, Swansea SA2 8PP, Wales, United Kingdom (e-mail: k.g.f.ahmeda.717828@swansea.ac.uk).

B. Benbakhti, S. J. Duffy, and W. Zhang are with Department of Electronics and Electrical Engineering, Liverpool John Moores University, Byrom Street, L3 3AF, Liverpool, England, United Kingdom.

A. Soltani is with LN2, University of Sherbrooke, Canada and IEMN, University of Lille, France.

II. ALGAN/GAN TLM HETEROSTRUCTURE

The studied epi-structure was grown by molecular beam epitaxy (MBE) on HP-Si [111] substrate with a thickness of $\sim$ 480 μm followed by a 1.7 μm $Al_{0.1}Ga_{0.9}N$ back-barrier layer, to reduce alloy scattering and to improve the carrier confinement in the 2DEG, followed by a 15 nm GaN channel. A 1 nm AlN spacer was used to reduce alloy disorder scattering and enhance electron mobility in the channel [8], followed by a 25 nm undoped $Al_{0.32}Ga_{0.68}N$ barrier and a 1 nm GaN cap layer. In an attempt to reduce the contact resistance, the source-to-drain terminal is formed by rapid thermal annealing of an evaporated Ti/Al/Ni/Au (10/200/40/100 nm) multilayer metallisation scheme at 870° C for 30 seconds under nitrogen atmosphere. The devices are electrically isolated by He^+ ion multiple implantations. To reduce trapping effects and dispersion, the surface of the devices are N_2O pre-treated for two minutes followed by SiO_2/Si_3N_4 (100/50 nm) bi-layer passivation, performed by plasma-enhanced chemical vapor deposition (CVD) at 340° C. The passivation layer is opened by using a CHF_3/CF_4 reactive ion etching plasma. Before taking any measurements, $V_{DS} = 0$ V is applied for a period of time, $t > 10$ seconds, to fully recover the device from the deleterious phenomena of charge trapping and self-heating that can distort further measurements. The trace of drain current is reproducible showing that no permanent degradation of the drain current occurs in experiment but only recoverable degradation, i.e., due to charge trapping and self-heating. The fabrication process flow is similar to that reported in Ref. [9] with Si_3N_4 passivation.

The spacing between the Ohmic contacts varies from L1 = 4 μm, L2 = 8 μm, L3 = 12 μm and L4 = 18 μm. The Ohmic contact length is LC = 50 μm for all the source-to-drain distances as depicted in Fig. 1(a). The energy band diagram overlapped with electron concentration profile in the heterostructure cross-section is illustrated in Fig. 1(b). The described Ti/Al/Ni/Au multilayer metallisation scheme was used for Ohmic contacts to create TLM heterostructures with

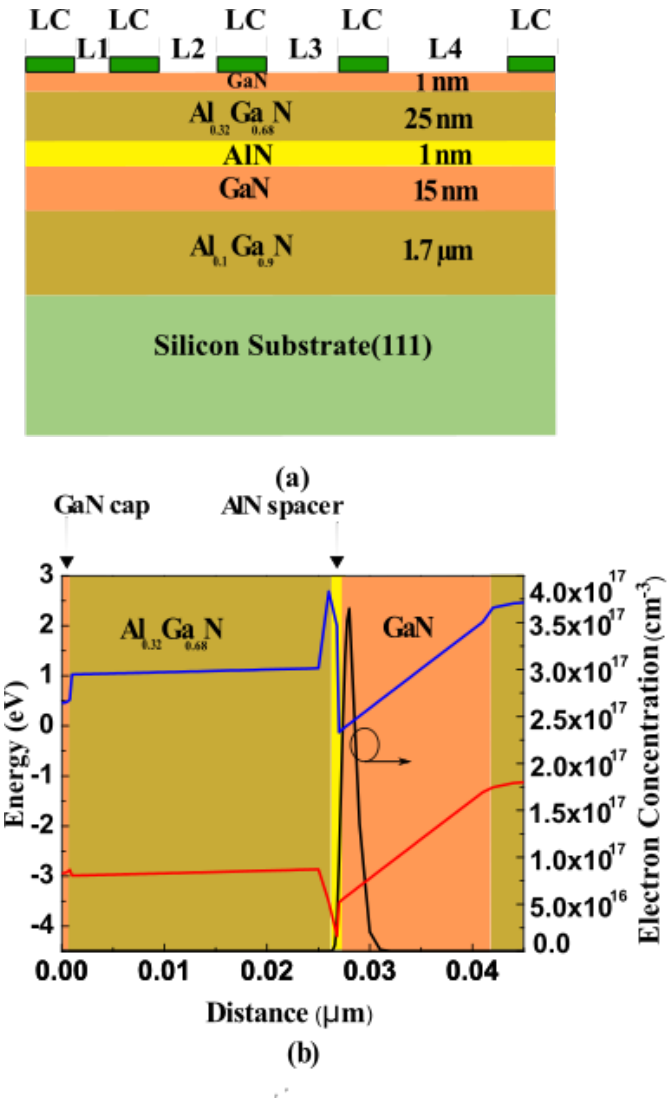

Fig. 1. (a) Schematic cross section of the AlGaN/GaN TLM structure and (b) energy band diagram and electron concentration profile at equilibrium.

various source-to-drain distances. Hall-effect measurements indicate a 2DEG electron mobility of 1950 $cm^2/V.s$, at room temperature. A C-V technique has revealed an electron sheet density of $n_s = 1.5 \times 10^{13}\ cm^{-2}$. The Ohmic contacts were implemented to the structures by using heavily doped GaN regions with a measured contact resistance of $0.3\ \Omega.mm$.

The I-V characteristics of the 100 μm wide TLM structures with the described source-to-drain distances plotted in Fig. 2 are measured at DC and dark conditions using Agilent B1500A framework. For the shortest distance of 4 μm, the voltage applied on the contact is restricted to 15 V to prevent contacts damage, while for other spacing lengths of 8 μm, 12 μm and 18 μm, the maximum applied voltage is set to 20 V. The arrows point to bias points at which a temperature is measured at the structure (18 μm and 4 μm TLM structures only) surface close to the drain.

III. SIMULATION METHODOLOGY FOR THE TLM STRUCTURE WITH VARIOUS SOURCE TO DRAIN DISTANCES

The electro-thermal model used to simulate electron transport in the TLM heterostructures combines two-dimensional (2D) drift-diffusion (DD) simulations with 2D heat transport model. In the calibration at a low electric field shown in Fig. 4(a), we have used a low-field electron mobility of 1950 $cm^2/V.s$, a saturation velocity of $1.9 \times 10^7\ cm/s$, [10] within the concentration dependent mobility model, and a contact resistance of $0.3\ \Omega.mm$. At a high electric field, a combination of the nitride specific field dependent mobility model [11] with Shockley-Read-Hall (SRH) recombination and Fermi-Dirac statistics is used. The Poisson and current continuity equations are solved self-consistency in all simulations [12].

Specifically, the low-field analytic mobility model based on Caughey and Thomas [13], [14] is employed in the simulation given be:

$$\mu_n(N, T_L) = \mu_{min}\left(\frac{T_L}{300}\right)^{\alpha} + \frac{\mu_{max}\left(\frac{T_L}{300}\right)^{\beta} - \mu_{min}\left(\frac{T_L}{300}\right)^{\alpha}}{1 + \left(\frac{T_L}{300}\right)^{\gamma}\left(\frac{N}{N_{crit}}\right)^{\delta}} \quad (1)$$

where N and T_L are the total doping concentration and the temperature in Kelvin, μ_{max} and μ_{min} are the mobility of undoped samples, where lattice scattering plays a dominant role and the mobility of highly doped materials, where impurity scattering is the main scattering mechanism. N_{crit} is the doping concentration when the mobility reaches the average value of μ_{max} and μ_{min}, δ is a measure of how quickly the mobility changes from μ_{max} and μ_{min}, δ , β and γ are temperature dependent coefficients.

The AlGaN/GaN TLM heterostructures have a background doping concentration of $1 \times 10^{16}\ cm^{-3}$. Carbon traps density of $1 \times 10^{17}\ cm^{-3}$ at an energy level $E_{TC} = E_V + 0.9eV$ and iron traps concentration of $4 \times 10^{18}\ cm^{-3}$ at $E_{TI} = E_V +$

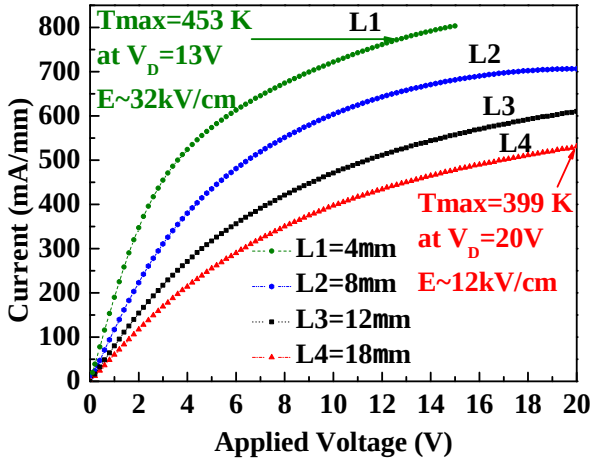

Fig. 2. DC I-V measured characteristics of the AlGaN/GaN TLM structures. The arrows indicate the bias at which temperature of the structure shown at the given electric field is measured at the surface.

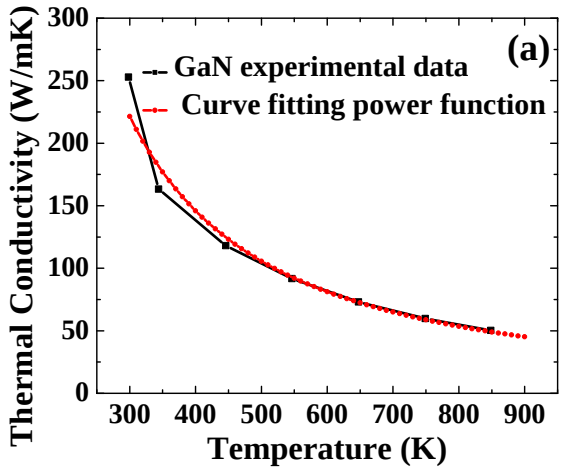

Fig. 3. Thermal conductivity of GaN (a) [21] and AlN (b) [22] as a function of temperature compared with a fitting power function.

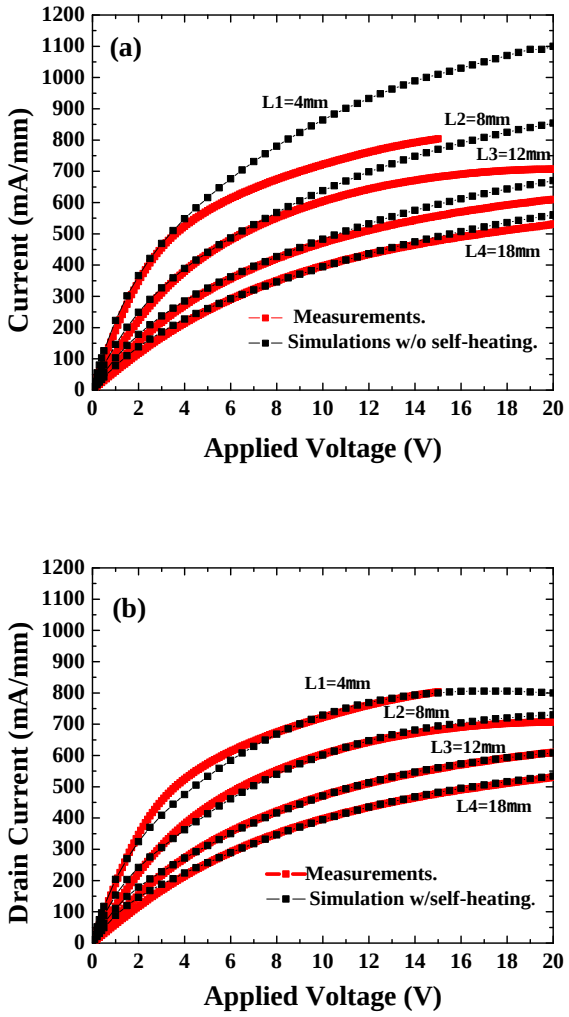

Fig. 4. I-V characteristics of AlGaN/GaN TLM structure: (a) DD simulations of the AlGaN/GaN TLM without a self-heating effect, (b) electro-thermal (ET) simulations of the AlGaN/GaN TLM (with a self-heating effect). Note that the mobility model in the DD and the ET simulations has been calibrated at a low-electric field only.

0.6 eV are considered in the GaN buffer and $Al_{0.1}Ga_{0.9}N$ back barrier, respectively [15]. HP-Si [111] substrate is a p-type doped [16] with a concentration density of 5×10^{18} cm^{-3}. The GaN cap donor concentration was set to be 5×10^{20} cm^{-3}, which is similar to that reported in [17] with an energy level of $E_T = E_C - 0.5$ eV [18]. We simulate a 8 μm thickness of the Si substrate with a bottom thermal contact at $T = 300$ K but do not introduce additional thermal resistance at the bottom of the simulated structure.

To investigate the impact of self-heating on the device performance, the temperature variations for different source-to-drain distances have been considered. The I-V characteristics of TLM structures are firstly simulated using the DD transport model without considering the self-heating effects to accurately calibrate the low-field mobility and saturation velocity [19] in the linear region of the device, where the self-heating effect is negligible.

Later, self-heating effect is taken into consideration to reproduce the output characteristics as shown in Fig. 4(b). The thermal modelling is activated by Giga module accounting for lattice heat flow in the device [20]. The used values of thermal conductivity of the different layers were taken from Refs. [21] and [22]. Giga module in Atlas [12] solves the lattice heat flow equation in addition to the DD and Poisson equations making the overall simulations to be electro-thermal. The heat flow equation is given by:

$$C\frac{\partial T_L}{\partial t} = \nabla(\kappa\nabla T_L) + H \tag{2}$$

where C denotes the heat capacitance per unit volume, κ is the thermal conductivity of the respective materials, H is the heat generation term, and T_L is the local lattice temperature. Thermal conductivity for GaN and AlN has been fit against measured experimental data as presented in Fig. 3. Here, we

TABLE I
THE FITTING COEFFICIENTS FOR GAN AND ALN USED IN THE RELATION (2). NOTE THAT THE COEFFICIENT α_κ HAS UNITS OF W/mK WHILE β_κ IS UNITLESS.

Materials	Coefficient (α_κ) (W/mK)	Coefficient (β_κ)
GaN	2.2132	1.447
AlN	2.83	1.529

have used a power function in the form:

$$\kappa(T_L) = \alpha_\kappa (\frac{T_L}{300})^{-\beta\kappa} \tag{3}$$

To fit a dependence of thermal conductivity on temperature with experimental data [21] for GaN and AlN [22] shown in Fig. 3, respectively, that have been used in the simulations. $\alpha\kappa$ and $\beta\kappa$ are the respective fitting coefficients for GaN and AlN summarized in Table I The heat generation term is given by the equation [20]:

$$H = \left[\frac{\left|\vec{j_n}\right|^2}{q\mu_n n} + \frac{\left|\vec{j_p}\right|^2}{q\mu_p p}\right] + q(R-G)[\phi_p - \phi_n + T_L(P_P - P_n)] - T_L(\vec{j_n}\nabla P_n + \vec{j_n}\nabla P_p) \tag{4}$$

where $|\vec{j_n}|$, $|\vec{j_p}|$ are the particle current densities of electrons and holes, μ_n, μ_p are the mobility of electrons and holes. n, p are the electron and hole concentrations; ϕ_n, ϕ_p are the Quasi-Fermi levels of electrons and holes; P_p, P_n are the thermoelectric powers of electrons and holes, R is the bulk recombination rate of carriers; G is the carrier generation rate; T_L is the local lattice temperature; and q is elementary charge of an electron.

IV. THE ROLE OF SELF-HEATING AND POLARIZATION

Fig. 4 shows the calibrated I-V characteristics with and without self-heating effect. Fig. 4(a) presents the calibration of the TLM structure against the experimental measurements without self-heating. A larger difference between the measurement results and the simulations, that is caused by self-heating effect, is seen for the shortest contact spacing of L1 = 4 μm at $V_{DS} = 20\ V$. The difference between the experimental measurements and the simulation data reduces when the source-to-drain distance increases. Fig. 4(b) compares the simulation results obtained from electro-thermal simulations, while using the calibration of thermal conductivity from Fig. 3. A stronger self-heating effect is observed for the shortest source-to-drain distance TLM, L1 = 4 μm, when compared with longest TLM, L4 = 18 μm. This is due to the higher electric field between the contacts in the shortest TLM compared with larger TLMs. The drain current reduction occurs due to mobility degradation caused by the self-heating. The simulation agreement improves as the distance between the source and drain is increased as expected so a very good agreement between simulation results and measurement data can be observed.

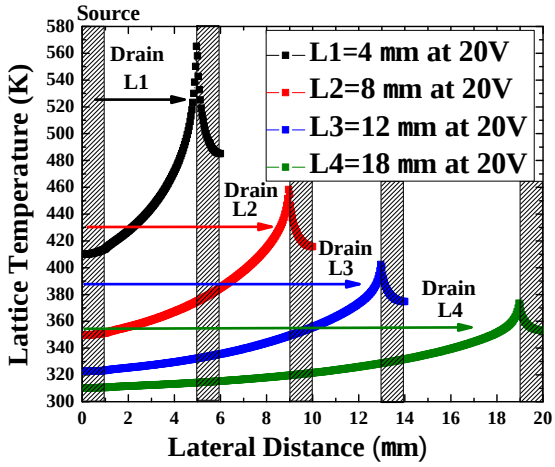

Fig. 5. Lattice temperature profiles in the 2DEG along the channel for different source-to-drain distances at $V_{DS} = 20\ V$.

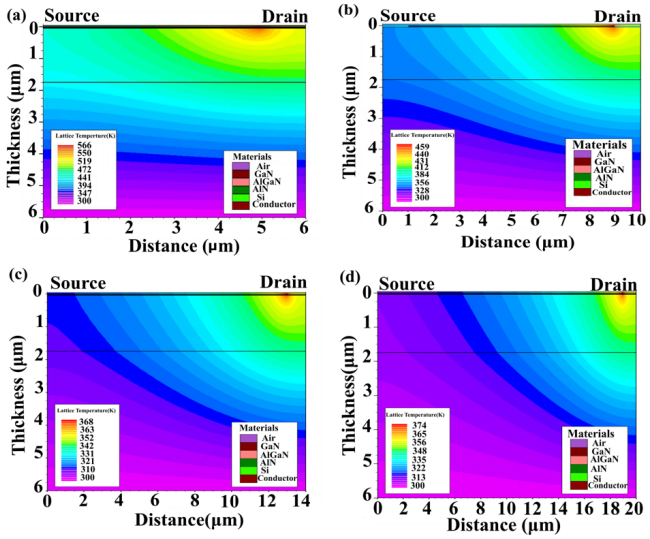

Fig. 6. 2D Lattice temperature distributions for TLM heterostructures with a source-to-drain distance of L1 = 4 μm (a), L2 = 8 μm (b), L3 = 12 μm (c) and L4 = 18 μm (d) at applied biases of 20 V (a, b, c, d), respectively.

The lattice temperature profiles in the 2DEG along the channel and its 2D distributions for all the structures (L1, L2, L3, and L4) are presented in Figs. 5 and 6, respectively. When the spacing between the source and the drain decreases, which increases the electric field at the vicinity of the drain [23] in a TLM structure, the lattice temperature increases and hence degrades the transport properties [24]. The GaN channel temperature increase is due to more energetic carriers in the channel with a larger kinetic energy accelerated by the increasing electric field [24]–[26]. The hot spot is located next to the drain contact for all structures [27]. At an applied drain-to-source bias of 20 V, the shortest structure (L1 = 4 μm) exhibits a peak lattice temperature of 566 K which is reported similarly in [25]. When the source-to-drain distance increases

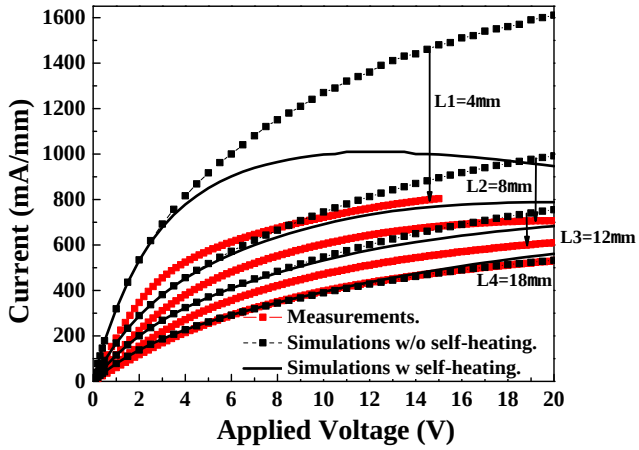

Fig. 7. Measured I-V characteristic of TLM structure (red lines) plotted against the hypothetical low-field calibrated results. The black dashed lines represent the simulations without self-heating while the black solid lines are the simulation results including self-heating effects. In all simulations, the polarization value of the largest structure (L4 = 18 μm) is used.

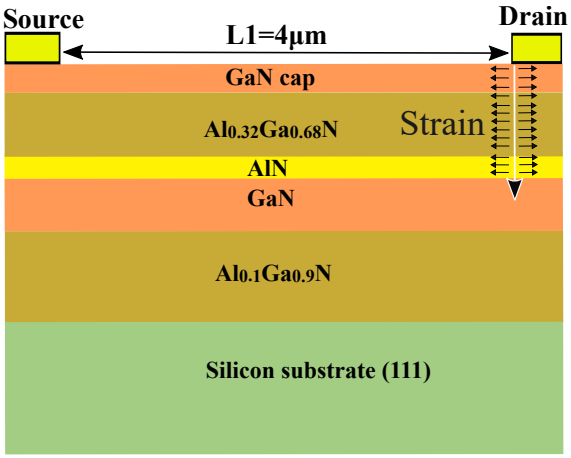

Fig. 8. Schematic diagram of the TLM structure that illustrates the strain induces by applied electrical stress.

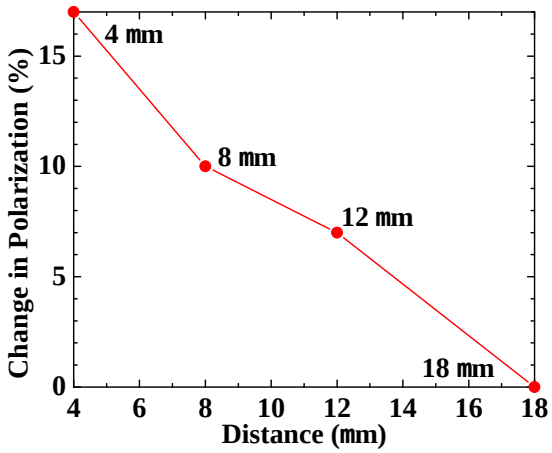

Fig. 9. The total polarization value decreases when compared to the total polarization used in the largest 18 μm TLM structure.

to 8 μm, a peak of lattice temperature decreases to 459 K in the structure (L2) and then to 403 K and to 374 K in the 12 μm and 18 μm structures (L3 and L4). The hot spot remains at the drain side for all TLM structures [28], [29]. The maximum simulated lattice temperature of 374 K at applied bias of 20 V in the 18 μm TLM structure is in a reasonable agreement ($\sim$ 7%) with a measured temperature of 399 K indicated in Fig. 2. In the smallest, 4 μm TLM structure, the simulations give a lattice temperature of 434 K at applied bias of 13 V (used in the experiment) which is also in a good agreement ($\sim$ 4%) with experimentally measured temperature of 453 K (Fig. 2).

The drain current in the largest TLM structure with a drain-source distance of L4 = 18 μm is compared against the scaled structures at an applied voltage V_{DS} = 15 V excluding and including the self-heating effects. The self-heating effect has a very small impact on the current of the 18 μm TLM structure. When the distance between the source and drain contacts is reduced to L3 = 12 μm, the drain current increases by 31.7 % (self-heating included) and by 40.7 % (self-heating excluded). Further scaling of the distance between the source and drain contact to L2 = 8 μm, the drain current increases by 61.7 % in the simulation with self-heating and 88 % without self-heating. Finally, for the shortest TLM structure of L1 = 4 μm, the drain current increases by 109.6 % with self-heating included and by 210.9 % with self-heating excluded in the simulation as compared to the largest TLM structure (L4 = 18 μm), which serves here as a reference to the comparison. When applying an external electrical stress on the TLM structure (applied voltage) via contacts, the wurtzite crystal structure of III-Nitrides suffers from the stress. This affects the polarization along with different spacing between the contacts. This phenomenon is known as the inverse or converse piezoelectric effect [29], [30].

To study this phenomenon, we altered the polarization factor for TLM structures to mimic the electrical stress that is applied after each measurement thus changing the total value of polarization. Fig. 7 illustrates hypothetical I-V characteristics if the polarization factor would be fixed at a value calibrated for the TLM structure with L4 = 18 μm, the largest source-to-drain distance. By applying this value on L1 = 4 μm, the drain current has increased by 66.8 % in the simulation, which clearly disagrees with experimental observations.

Electrical and mechanical strain/stress and its relationship with the electric field in GaN HEMTs has a tremendous impact on GaN based devices in general [29]. Nitride materials like GaN which have unique properties due to the lack of inversion symmetry and high iconicity exhibit inverse/converse piezoelectric effect due to strain/stress generated by the electric field [31]. When applying an external electrical and mechanical stress on the TLM structure via contacts (applied voltage), the wurtzite crystal structure of III-Nitrides suffers

distortion and deformation from mechanical stress on GaN and AlGaN layers. This affects the polarization along with different spacing between the contacts. The electrical stress caused by an applied voltage on Ohmic contacts induces a lattice deformation at the vicinity of the drain as illustrated in Fig. 8. The total polarization value decreases when compared to the largest contact of 18 μm for 12 μm, 8 μm, and 4 μm by 7 %, 10 %, and 17 %, respectively. The relationship between the change-in-polarization and the source-to-drain distance is almost linear, as shown in Fig 9.

V. Conclusions

We have studied $Al_{0.32}Ga_{0.68}N$/AlN/GaN/$Al_{0.1}Ga_{0.9}N$ TLM heterostructures with a GaN cap layer grown on a p-type doped HP-Si [111] substrate. Their I-V characteristics from experimental measurements were simulated via a 2D drift-diffusion transport model using Fermi-Dirac statistics and the SRH recombination model by commercial tool Atlas-Silvaco [12]. Thermal model was employed to study the self-heating effects with the thermal conductivity approximated by a power function and calibrated to experimental data. We have found that the current soon becomes limited by increase in a lattice temperature with the increase in applied bias up to 13% (the 4 μm structure) and that this limitation occurs sooner in shorter structures. We have demonstrated a good agreement of the electro-thermal simulations predicting a lattice temperature of 374 K against experimental temperature of 399 K at applied bias of 20 V in the largest, 18 μm structure as well as in the smallest, 4 μm structure, predicting a lattice temperature of 434 K against experimental temperature of 453 K at applied bias of 13 V. The maximum lattice temperature (for instance $\sim 566K$ in the 4 μm structure at $V_{DS} = 20$ V was predicted in the vicinity of the drain. In addition, we have observed that, by applying electrical stress (voltage) on the Ohmic contacts, the total polarization value in heterostructure reduces when compared to the largest contact distance of 18 μm for 12 μm, 8 μm, and 4 μm by 7 %, 10 %, and 17%, respectively. This decrease in the total polarization is due to the inverse piezoelectric effect, or also called the converse piezoelectric effect, caused by the additional stress induced by the applied electric field on contact. The inverse piezoelectric effect changes the total polarization thus affecting a 2DEG density in the channel [29], [30], [32].

References

[1] M. U. Ishida, Y. Ueda, T. Tanaka, and T. Ueda, GaN power switching devices, in *P*roc. Int. Power Eng. Conf. (IPEC), 2010, pp. 1014-1017.

[2] R. J. Trew, High-frequency solid-state electronic devices, *IEEE Trans. Electron Devices*, vol. 52, no. 5, pp. 638-649, May. 2005.

[3] R. Vetury, N. Q. Zhang, S. Keller, and U. K. Mishra, The impact of surface states on the DC and RF characteristics of AlGaN/GaN HFETs, *IEEE Trans. Electron Devices* vol. 48, no. 3, pp. 560-566, Mar. 2001.

[4] E. A. Jones, F. F. Wang, and D. Costinett, Review of Commercial GaN Power Devices and GaN-Based Converter Design Challenges, *IEEE J. Emer. Sel. Topics Power Electron.*, vol. 4, no. 3, pp. 707-719, Sept. 2016.

[5] S. L. Delage and C. Dua, Wide band gap semiconductor reliability: Status and trends, *Microelectron. Reliab*, vol. 43, no. 9, pp. 1705-1712, Sept. 2003.

[6] H. Tao, W. Hong, B. Zhang, and X. Yu, A Compact 60W X-Band GaN HEMT Power Amplifier MMIC, *IEEE Microw. Wireless Compon. Lett.*, vol. 27, no. 1, Jan. 2017.

[7] S. Taking, AlN/GaN MOS-HEMTs Technology, PhD Thesis, Division Electronics Nanoscale Eng., School Eng., Uni. Glasgow, Glasgow, UK, 2012.

[8] I. P. Smorchkova, L. Chen, T. Mates, L. Shen, S. Heikman, B. Moran, S. Keller, S. P. DenBaars, J. S. Speck, and U. K. Mishra, AlN/GaN and (Al,Ga)N/AlN/GaN two-dimensional electron gas structures grown by plasma-assisted molecular-beam epitaxy, *J. Appl. Phys*, vol. 90, no. 10, pp. 5196, Nov. 2001.

[9] A. Soltani, J. C. Gerbedoen, Y. Cordier, D. Ducatteau, M. Rousseau, M. Chmielowska, M. Ramdani, and J. C. De Jaeger, Power Performance of AlGaN/GaN High-Electron-Mobility Transistors on (110) Silicon Substrate at 40 GHz, *IEEE Electron Device Lett*, vol. 34, no. 4, pp. 490-492, Apr. 2013.

[10] S. Bajaj, O. F. Shoron, P. S. Park, S. Krishnamoorthy, F. Akyol, T. Hung, S. Reza, E. M. Chumbes, J. Khurgin, and S. Rajan,Density-dependent electron transport and precise modeling of GaN high electron mobility transistors, *Appl. Phys. Lett*, vol. 107, no. 15, pp. 153504, Oct. 2015.

[11] M. Farahmand, C. Garetto, E. Bellotti, K. F. Brennan, M. Goano, E. Ghillino, G. Ghione, J. D. Albrecht, and P. P. Ruden, Monte Carlo simulation of electron transport in the III-nitride wurtzite phase materials system: binaries and ternarie, *IEEE Trans. Electron Devices*, vol. 48, no.3, pp. 535-542, Mar. 2001.

[12] Silvaco, Atlas Users Manual, Device Simulation Software, 2016 ed., Silvaco Int, Santa Clara, CA. 2016.

[13] D. Caughey and R. Thomas, Carrier mobilities in silicon empirically related to doping and field, *IEEE. Proc*, vol. 55, no. 12, pp. 21922193, Dec. 1967.

[14] S. Selberherr, Process and device modeling for VLSI, *Microelectron. Reliab* , vol. 24, no. 2, pp. 22557, 1984.

[15] M. J. Uren, J. Mreke, and M. Kuball,Buffer Design to Minimize Current Collapse in GaN/AlGaN HFETs, *IEEE Trans.Electron Devices*, vol. 59, no.12, pp. 3327-3333, Dec. 2012.

[16] E. M. Chumbes, A. T. Schremer, J. A. Smart, Y. Wang, N. C. MacDonald, D. Hogue, J. J. Komiak, S. J. Lichwalla, R. E. Leoni, and J. R. Shealy, AlGaN/GaN high electron mobility transistors on Si(111) substrates, *IEEE Trans.Electron Devices*, vol. 48, no. 3, pp. 420-426, Mar. 2001.

[17] J. Kuzmik, C. Ostermaier, G. Pozzovivo, B. Basnar, W. Schrenk, J. F. Carlin, M. Gonschorek, E. Feltin, N. Grandjean, Y. Douvry, C. Gaquiere, J. C. De Jaeger, K. Čičo, K. Fr´ohlich, J. Škriniarova, J. Kovač, G. Strasser, D. Pogany, and E. Gornik, Proposal and Performance Analysis of Normally Off n++ GaN/InAlN/AlN/GaN HEMTs With 1-nm-Thick InAlN Barrier, *IEEE Trans. Electron Devices*, vol. 57, no. 9, pp. 2144-2154, Sept. 2010.

[18] Y. Lin, Q. Ker, C. Ho, H. Chang, F. Chien, Nitrogen-vacancy-related defects and Fermi level pinning in n-GaN Schottky diode, *J. Appl. Phys*, vol. 94, no. 3, pp. 1819-1822, Aug. 2003.

[19] B. E. Foutz, S. K. OLeary, M. S. Shur, and L. F. Eastman, Transient electron transport in wurtzite GaN, InN, and AlN, *J. Appl. Phys*, vol. 85, no. 11, pp. 7727-7734, Jun. 1999.

[20] G. K. Wachutka, Rigorous thermodynamic treatment of heat generation and conduction in semiconductor device modeling, *IEEE Trans. Comput-Aided Design Integr. Circuits Syst*, vol. 9, no. 11, pp. 1141-1149, Nov. 1990.

[21] V. Palankovski and R. Quay, *Analysis and Simulation of Heterostructure Devices*, Springer-Verlag Wien, 2004, pp. 44-45.

[22] H. Shibata, Y. Waseda, H. Ohta, K. Kiyomi, K. Shimoyama, K. Fujito, H. Nagaoka, Y. Kagamitani, R. Simura, and T. Fukuda, High Thermal Conductivity of Gallium Nitride (GaN) Crystals Grown by HVPE Process, *Mater. Trans*, vol. 48, no. 10, pp. 2782 2786, Sept. 2007.

[23] S. Rajasingam, J. W. Pomeroy, M. Kuball, M. J. Uren, T. Martin, D. C. Herbert, K. P. Hilton, and R. S. Balmer,Micro-Raman Temperature Measurements for Electric Field Assessment in Active AlGaNGaN HFETs, *IEEE Electron Device Lett*, vol. 25, no. 7, Jul. 2013.

[24] B. Benbakhti, A. Soltani, K. Kalna, M. Rousseau, and J. C. De Jaeger, Effects of Self-Heating on Performance Degradation in AlGaN/GaN Based Devices, *IEEE Trans. Electron Devices*, vol. 56, no. 10, pp. 2178-2185, Oct. 2009.

[25] W. H. Tham, D. S. Ang, L. Kanta Bera, S. B. Dolmanan, T. N. Bhat, V. K. Lin, and S. Tripathy, Comparison of the AlxGa1xN/GaN Heterostructures Grown on Silicon-on-Insulator and Bulk-Silicon Substrates, *IEEE Trans. Electron Devices*, vol. 63, no. 1, Jan. 2016.

[26] M. Faqir, G. Verzellesi, G. Meneghesso,E. Zanoni, and F. Fantini, Investigation of High-Electric-Field Degradation Effects in AlGaN/GaN HEMTs, *IEEE Trans. Electron Devices*, vol. 55, no. 7, Jul. 2008.

[27] T. Sadi, R. W. Kelsall, and N. J. Pilgrim, Investigation of Self-Heating Effects in Submicrometer GaN/AlGaN HEMTs Using an Electrothermal Monte Carlo Method, *IEEE Trans.Electron Devices*, vol. 53, no. 12, pp. 2892-2900, Dec. 2006.

[28] J. Kuzmk, M. Tapajna, L. Vlik, M. Molnr, D. Donoval, C. Fleury, D. Pogany, G. Strasser, O. Hilt, F. Brunner, and J. Wrfl, Self-Heating in GaN Transistors Designed for High-Power Operation, *IEEE Trans. Electron Devices*, vol. 61, no. 10, Oct. 2014.

[29] U. Chowdhury, J. L. Jimenez, C. Lee, E. Beam, P. Saunier, T. Balistreri, S. Park, T. Lee, J. Wang, M. J. Kim, J. Joh, and J. A. d. Alamo, TEM Observation of Crack- and Pit-Shaped Defects in Electrically Degraded GaN HEMTs, *IEEE Electron Device Lett.*, vol. 29, no. 10, pp. 1098-1100, Oct. 2008.

[30] R. Chu, Gate-Recessed GaN High Electron Mobility Transistors with Scaled Gate Length, PhD dissertation, Dept. Elec. Electronics Eng., Uni. California, Santa Barbara, Dec. 2008.

[31] D. Sztenkiel, M. Foltyn, G.P. Mazur, R. Adhikari, K. Kosiel, K. Gas, M. Zgirski, R. Kruszka, R. Jakiela,T. Li, A. Piotrowska, A. Bonanni, M. Sawicki and T. Dietl, Stretching Magnetism with an Electric Field in a Nitride Semiconductor, *Nat. Commun.*, vol. 7, art. no. 13232, Oct. 2016.

[32] J. Joh, L. Xia, and J. A. d. Alamo, Gate Current Degradation Mechanisms of GaN High Electron Mobility Transistors, *in IEDM Tech. Dig*, Dec. 2007, pp. 385-388.